

Infrared Properties of Radio-Selected Submillimeter Galaxies in the Spitzer First Look Survey Verification Field

D. T. Frayer¹, S. C. Chapman², L. Yan¹, L. Armus¹, G. Helou¹, D. Fadda¹, R. Morganti³, M. A. Garrett⁴, P. Appleton¹, P. Choi¹, F. Fang¹, I. Heinrichsen¹, M. Im⁵, M. Lacy¹, F. Marleau¹, F. J. Masci¹, D. L. Shupe¹, B. T. Soifer¹, G. K. Squires¹, L. J. Storrie-Lombardi¹, J. A. Surace¹, H. I. Teplitz¹, G. Wilson¹

ABSTRACT

We report on submillimeter and infrared observations of 28 radio-selected galaxies in the *Spitzer* First Look Survey Verification field (FLSV). All of the radio-selected galaxies that show evidence for emission at $850\mu\text{m}$ with SCUBA have *Spitzer* counterparts at $24\mu\text{m}$, while only half of the radio-selected galaxies without $850\mu\text{m}$ emission have detectable counterparts at $24\mu\text{m}$. The data show a wide range of infrared colors ($S70/S24 < 5\text{--}30$, $S8/S3.6 < 0.3\text{--}4$), indicative of a mixture of infrared-warm AGN and cooler starburst dominated sources. The galaxies showing $850\mu\text{m}$ emission have *Spitzer* flux densities and flux density ratios consistent with the range of values expected for high-redshift ($z = 1\text{--}4$) ultraluminous infrared galaxies.

Subject headings: galaxies: active — galaxies: evolution — galaxies: formation — galaxies: starburst

1. Introduction

The *Spitzer Space Telescope* provides us with the exciting opportunity to study the high-redshift universe at mid&far-infrared wavelengths. The *IRAS* mission first uncovered the presence of infrared luminous galaxies in the local universe (Neugebauer et al. 1984), and the sub-mm/mm surveys with SCUBA and MAMBO have highlighted the importance of ultraluminous infrared galaxies (ULIRGs, $> 10^{12} L_{\odot}$) at high redshift (e.g., Smail, Ivison, & Blain 1997; Hughes et al. 1998; Bertoldi et al. 2000). Studies of high-redshift ULIRGs are important for our general understanding of galaxy evolution since they are responsible for a significant fraction of the total energy generated by all galaxies over the history of the universe (e.g., Blain et al. 2002).

¹Spitzer Science Center, California Institute of Technology 220–06, Pasadena, CA 91125, USA

²California Institute of Technology 320–47, Pasadena, CA 91125, USA

³ASTRON, Dwingeloo, The Netherlands

⁴JIVE, Dwingeloo, The Netherlands

⁵Astronomy Program, SEES, Seoul National University, Seoul, Korea

The recent spectroscopic studies of the sub-mm galaxy (SMG) population show that the redshift distribution peaks at $z \sim 2-3$ (Chapman et al. 2003b, 2004), and that the population is comprised of starbursts, AGN, and composite AGN+starburst systems (Ivison et al. 1998, 2000; Frayer et al. 2003; Knudsen, van der Werf, & Jaffe 2003). Even though many SMGs show the presence of AGN, the molecular CO line emission (Frayer et al. 1998, 1999; Neri et al. 2003) and X-ray data (Alexander et al. 2003) are consistent with the majority of the infrared emission for the population arising from star formation. The Multiband Imaging Photometer for *Spitzer* (MIPS, Rieke et al. 2004) allows us to directly measure the infrared colors and constrain the fraction of infrared-warm AGN dominated versus infrared-cool starburst dominated SMGs.

2. Observations

Before the launch of *Spitzer*, we identified potential SMGs in the First Look Survey Verification field (FLSV) by selecting radio sources with faint optical counterparts, following previous successful selection techniques (e.g., Cowie, Barger, & Kneib 2002; Chapman et al. 2003a). We used deep Westerbork 1.4 GHz radio data (rms= $9\mu\text{Jy}$, Morganti et al. 2004) and deep optical NOAO *R*-band data ($3\sigma = 26.4\text{ mag}$, Fadda et al. 2004a) to derive a list of candidate sources for follow-up observations with SCUBA. In the Spring of 2003, we observed 28 galaxies at the James Clerk Maxwell Telescope (JCMT) using the SCUBA two-bolometer photometry mode, achieving rms levels of 2–3 mJy at $850\mu\text{m}$.

The *Spitzer* observations were taken as part of the Extragalactic First Look Survey (FLS)¹. The 28 galaxies in the sample are located within the 0.25 degree² of the FLS verification field (FLSV) and were observed with both the InfraRed Array Camera (IRAC, Fazio et al. 2004) and MIPS. The data presented here have effective integration times of 480 s, 336 s, 168 s, and 34 s for the IRAC bands and the MIPS 24, 70, and $160\mu\text{m}$ arrays, respectively. The data were reduced using the standard SSC pipeline and were coadded and corrected offline as needed. The details of the data reduction will be described in future FLS data papers (IRAC: Lacy et al. 2004; MIPS-24 μm : Fadda et al. 2004b; MIPS-70,160 μm : Frayer et al. 2004b).

3. Results and Discussion

3.1. Source Identification

We observed 28 Westerbork radio sources with SCUBA and detected 7 SMGs at $S/N > 3$. Fourteen sources were not detected at $850\mu\text{m}$, and the remaining 7 sources have marginal results, showing positive signals of $1.5-3\sigma$ (Column [4], Table 1). The Westerbork radio data have a resolu-

¹*Spitzer* program ID = 26, <http://ssc.spitzer.caltech.edu/fls/extragal/spitzer.html>.

tion of $14'' \times 11''$ which is well matched to the SCUBA data, but is not sufficient to obtain reliable counterparts in general for the optical and *Spitzer* data. We used the higher resolution ($5''.0$) VLA (1.4 GHz) data of the field (Condon et al. 2003) to obtain more accurate radio positions. The resolution of the VLA data is well matched to the MIPS-24 resolution of $6''$. Although the VLA data have lower S/N ($\text{rms} \sim 20 \mu\text{Jy}$), the Westerbork sources were typically detected at $\gtrsim 3\sigma$ in the VLA image, providing radio positional errors of about $1\text{--}2''$. The offsets between radio and MIPS-24 positions are typically less than $2''$, consistent within the positional uncertainties of the radio data and the $1.5\text{--}2''$ positional uncertainties of the MIPS-24 data set. Based on the $24\mu\text{m}$ counts in the FLS field (Marleau et al. 2004), the probability of a chance coincidence within $2''$ is only about 1% for $24\mu\text{m}$ sources brighter than $100\mu\text{Jy}$. Hence, confusion at $24\mu\text{m}$ is not a significant issue for this study. After the identification of the MIPS-24 and R-band counterparts based on the radio positions, the corresponding MIPS-24 and optical positions were used to identify the appropriate IRAC counterparts.

Four of the Westerbork sources have multiple radio components at the resolution of the VLA data (1, 45, 79, 128). Source 1 is the brightest *Spitzer* source and is comprised of five components, all detected in the MIPS-24, R-, and the IRAC-bands. The details of the source identification are provided in Table 1. Figure 1 shows the MIPS-24 and IRAC-3.6 images for the 7 SMGs detected at $850\mu\text{m}$ with $\text{S/N} > 3$.

All 14 sources showing $850\mu\text{m}$ emission above the 1.5σ level have $24\mu\text{m}$ counterparts, although source 208 is only detected at about the $2.5\text{--}3\sigma$ level at $24\mu\text{m}$. The detection of $24\mu\text{m}$ counterparts associated even with the marginal $850\mu\text{m}$ sources gives credence to the reliability of the $> 3\sigma$ SMG sources. In comparison for the 14 radio sources without SCUBA detections, only half have $24\mu\text{m}$ counterparts. The detection of $24\mu\text{m}$ counterparts for this sample of radio-selected SMGs is consistent with the high fraction of $24\mu\text{m}$ counterparts found for the MAMBO and SCUBA sources in the Lockman Hole (Ivison et al. 2004; Egami et al. 2004).

Seven sources in the full sample do not have optical counterparts down to $R = 26.4$ mag, and only three are not detected by IRAC. The only source without any optical or IRAC counterpart is source 108 which is the brightest radio galaxy in the sample (likely a radio-loud AGN). Two sources (199 [$z = 1.06$] & 150 [$z = 0.84$]) in the sample have spectroscopic redshifts from the ongoing Keck DEIMOS redshift survey (Choi et al. 2004). The low redshift of $z = 1.06$ for the $850\mu\text{m}$ source 199 implies a cool dust temperature of 20 K assuming a temperature dependent sub-mm to radio redshift relationship (Blain 1999).

3.2. Infrared Properties

The MIPS $24\mu\text{m}$ flux densities for the galaxies detected at $850\mu\text{m}$ are consistent with expectations, assuming standard ULIRG spectral energy distributions (SEDs) at the typical redshifts of $z \sim 2\text{--}3$ found for the SMG population (Chapman et al. 2003b; 2004). Figure 2 shows a range

of $S_{24}/S(1.4\text{GHz})$ flux density ratios for the population that may reflect a wide distribution of infrared colors. All of the galaxies showing $850\mu\text{m}$ emission lie within the range of values expected for local ULIRGs redshifted to $z = 1\text{--}4$. Galaxies without $850\mu\text{m}$ emission show a wider range of $S_{24}/S(1.4\text{GHz})$ flux density ratios. About half of the radio sources without detectable $850\mu\text{m}$ emission have properties consistent with ULIRGs, while the other half show excess radio emission compared to their $24\mu\text{m}$ emission, consistent with different degrees of radio-loudness.

MIPS $70\mu\text{m}$ observations can constrain the infrared colors of the SMGs. Infrared-warm, AGN dominated sources are expected to have flux density ratios of $S_{70}/S_{24} \sim 5$, while starburst dominated, infrared-cool sources are expected to have ratios of $S_{70}/S_{24} \gtrsim 10$. We only detect two sources at $70\mu\text{m}$, both of which are cool in the infrared (source 1: $S_{70}/S_{24} = 11$ and source 47: $S_{70}/S_{24} = 26$). To derive an estimated average S_{70}/S_{24} ratio for the SMG population, we coadded the $70\mu\text{m}$ data at the radio positions for the sources showing $850\mu\text{m}$ emission. We find an upper-limit of $S_{70} < 1.2\text{mJy}$ (2σ). This corresponds to an infrared color of $S_{70}/S_{24} < 5$, leaving out the two sources with $70\mu\text{m}$ detections. Including the two $70\mu\text{m}$ detections, the average ratio for the SMG population is $S_{70}/S_{24} < 7$, which is slightly lower than expected if the population is dominated by star-formation. Taken at face-value, these results could suggest that many SMGs are infrared-warm AGN, contrary to previous conclusions that the population is dominated by star-formation. However, the lower than expected S_{70}/S_{24} ratios may arise from strong $7.7\mu\text{m}$ PAH emission redshifted into the $24\mu\text{m}$ band, given that the median redshift for the SMG population is $z \sim 2.4$ (Chapman et al. 2003b; 2004).

The SEDs in the IRAC bands can be used to estimate redshifts from the rest-frame $1.6\mu\text{m}$ peak expected for star-forming systems (e.g., Egami et al. 2004) and to help identify AGN showing hot dust implied by their red IRAC colors (e.g., Ivison et al. 2004). For sources showing a significant bump in the IRAC bands, the implied redshifts are generally consistent (Column [11]&[12], Table 1) with the redshift estimates derived from the sub-mm to radio spectral index (Carilli & Yun 1999; Blain 1999). The discrepant photometric redshifts for sources 48&119 may indicate cool dust temperatures ($T_d < 40\text{K}$) for these SMGs.

Of the sources with $850\mu\text{m}$ emission and IRAC detections, only source 47 shows a strong increase in flux density as a function of wavelength across the IRAC bands consistent with an AGN. However, source 47 also has the highest S_{70}/S_{24} ratio in the sample ($S_{70}/S_{24}=26$), suggesting that it is likely an infrared-cool starburst that could be at $z \gtrsim 4$ and/or be highly reddened due to dust extinction. Hence, IRAC colors are not always conclusive for determining the properties at longer infrared wavelengths.

3.3. Extremely Red Objects

A significant fraction of SMGs is comprised of extremely red objects (EROs) (Smail et al. 1999; Frayer et al. 2004a). The ERO definition of $R - K > 6$ (Thompson et al. 1999) corresponds

to a flux density ratio of $S_{3.6}/S(R) \geq 85$. Using this criterion, we identify 8 EROs (Fig. 3). The 30% (8/27) fraction of EROs in this sample is larger than the 8% found for the total micro-Jy radio population (Smail et al. 2002), presumably since the SCUBA targets in this sample were generally selected on the basis of being faint and red in the optical bands. Figure 3 shows a wide range of IRAC colors for the SMG population, and no correlation is observed between the IRAC colors and the $R - [3.6]$ colors. Another interesting result is that most of the radio-selected EROs without detectable $850\mu\text{m}$ emission (6/7) are bright at $24\mu\text{m}$, indicating that these sources are infrared-bright galaxies (likely high-redshift ULIRGs) below the current SCUBA detection limits.

4. Conclusions

All of the radio-selected SMGs in the sample have *Spitzer* counterparts, showing a wide range of infrared colors consistent with ULIRGs at $z = 1-4$. The combination of accurate radio positions and $24\mu\text{m}$ detections is a powerful tool for the identification of SMGs. More sensitive observations are required in the MIPS-70 and MIPS-160 bands to measure the infrared colors of the SMG population. In addition, observations with the *Spitzer* InfraRed Spectrograph are needed to determine the level at which PAH emission contributes to the MIPS-24 flux densities and to help determine the AGN fraction of the population. In general, *Spitzer* selected ULIRGs will be biased toward AGN, except within specific redshift bins associated with the PAH features which may be biased toward starbursts.

We thank the staff at the JCMT and the *Spitzer* Science Center for their support of these observations. This work is based in part on observations made with the *Spitzer Space Telescope*, which is operated by the Jet Propulsion Laboratory, California Institute of Technology under NASA contract 1407.

REFERENCES

- Alexander, D. M., et al. 2003, AJ, 125, 383
- Bertoldi, F., et al. 2000, A&A, 360, 92
- Blain, A. W. 1999, MNRAS, 309, 955
- Blain, A. W., Smail, I., Ivison, R. J., Kneib, J.-P., & Frayer, D. T. 2002, Physics Reports, 369, 111
- Carilli, C. L., & Yun, M. S. 1999, ApJ, 513, L13
- Chapman, S. C. et al. 2003a, ApJ, 585, 57
- Chapman, S. C., Blain, A. W., Ivison, R. J., Smail, I. R. 2003b, Nature, 422, 695
- Chapman, S. C., Blain, A. W., Ivison, R. J., Smail, I. R. 2004, ApJ, submitted
- Choi, P., et al. 2004, in preparation

- Condon, J. J., Cotton, W. D., Yin, Q. F., Shupe, D. L., Storrie-Lombardi, L. J., Helou, G., Soifer, B. T., Werner, M. W. 2003, *AJ*, 125, 2411
- Cowie, L. L., Barger, A. J., & Kneib, J.-P. 2002, *AJ*, 123, 2197
- Egami, E. et al. 2004, *ApJS*, this issue
- Fadda, D., Jannuzi, B., Ford, A., & Storrie-Lombardi, L. J. 2004a, *AJ*, in press (astro-ph/0403490)
- Fadda, D., et al., 2004b, in preparation
- Fazio, G. T., et al. 2004, *ApJS*, this issue
- Frayser, D. T., Armus, L., Scoville, N. Z., Blain, A. W., Reddy, N. A., Ivison, R. J., & Smail, I. 2003, *AJ*, 126, 73
- Frayser, D. T., et al. 2004b, in preparation
- Frayser, D. T., et al. 1999, *ApJ*, 514, L13
- Frayser, D. T., Ivison, R. J., Scoville, N. Z., Yun, M., Evans, A. S., Smail, I., Blain, A. W., & Kneib, J.-P. 1998, *ApJ*, 506, L7
- Frayser, D. T., Reddy, N. A., Armus, L., Blain, A. W., Scoville, N. Z., & Smail, I. 2004a, *AJ*, 172, 728
- Hughes, D., et al. 1998, *Nature*, 394, 241
- Ivison, R. J., Smail, I., Barger, A. J., Kneib, J.-P., Blain, A. W., Owen, F. N., Kerr, T. H., & Cowie, L. L. 2000, *MNRAS*, 315, 209
- Ivison, R. J., Smail, I., Le Borgne, J.-F., Blain, A. W., Kneib, J.-P., Bézecourt, J., Kerr, T. H., & Davies, J. K. 1998, *MNRAS*, 298, 583
- Ivison, R. J., et al. 2004, *ApJS*, this issue
- Knudsen, K. K., van der Werf, P. P., & Jaffe, W. 2003, *A&A*, 411, 343
- Lacy, M., et al. 2004, in preparation
- Marleau, F., et al., 2004, *ApJS*, this issue
- Morganti, R., et al., 2004, in preparation
- Neri, R., et al. 2003, *ApJ*, 597, L113
- Neugebauer, G., et al. 1984, *ApJ*, 278, L1
- Rieke, G., et al. 2004, *ApJS*, this issue
- Smail, I., Ivison, R. J., & Blain, A. W. 1997, *ApJ*, 490, L5
- Smail, I., Ivison, R. J., Kneib, J.-P., Cowie, L. L., Blain, A. W., Barger, A. J., Owen, F. N., & Morrison, G. 1999, *MNRAS*, 308, 1061
- Smail, I., Owen, F. N., Morrison, G. E., Keel, W. C., Ivison, R. J., & Ledlow, M. J. 2002, *ApJ*, 581, 844

Thompson, D., et al. 1999, ApJ, 523, 100

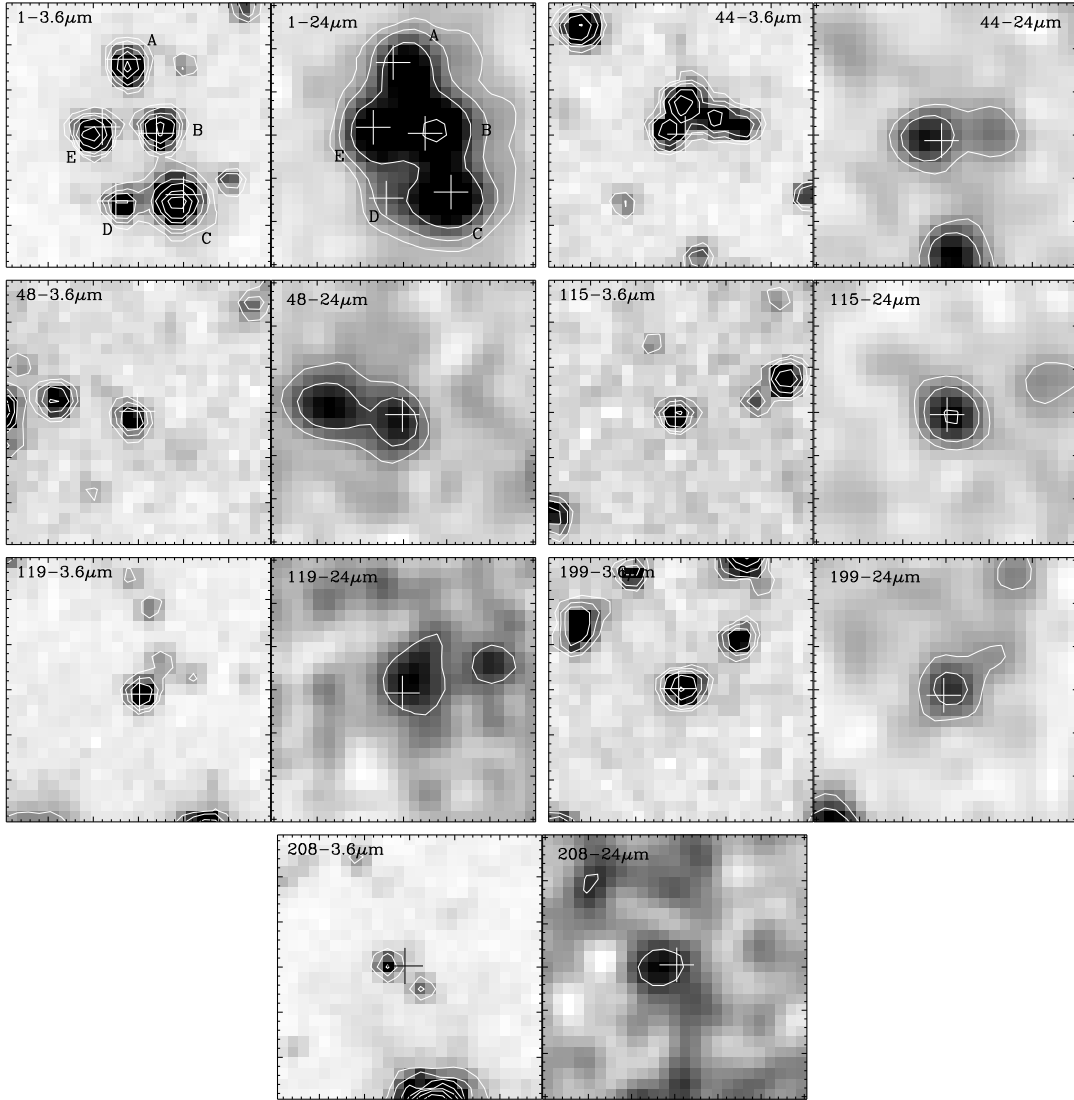


Fig. 1.— IRAC-3.6 μ m and MIPS-24 μ m images of the seven SMGs detected at 850 μ m with $S/N > 3$. Each panel is approximately 30'' in size (north is up and east is left) with tickmarks every 1''. The grey-scale is plotted on a logarithmic scale, and the contours start at 3σ and increase by factors of 2. The crosses represent the positions of the radio counterparts.

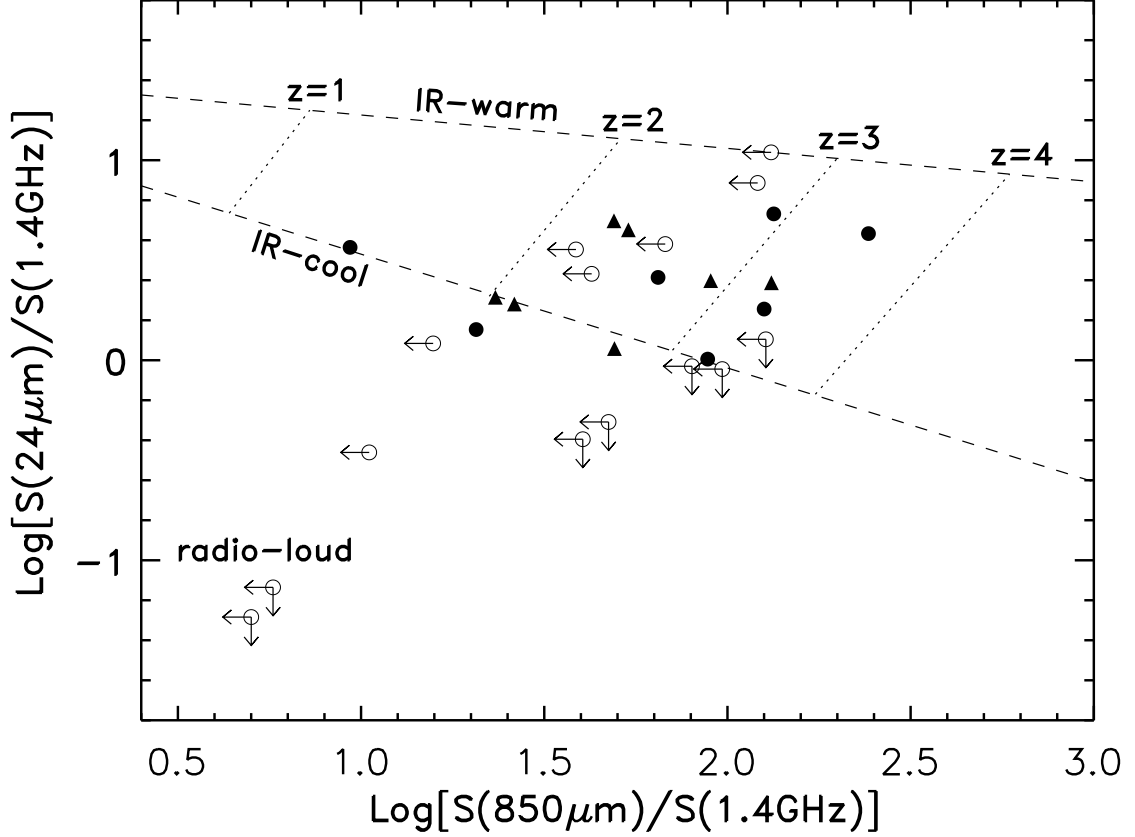


Fig. 2.— The $S_{24}/S(1.4\text{ GHz})$ flux density ratios as a function of the $S_{850}/S(1.4\text{ GHz})$ flux density ratio. The solid circles are the $> 3\sigma$ SMGs, the open circles are the radio sources without $850\mu\text{m}$ emission, and the solid triangles are the sources with $850\mu\text{m}$ measurements of $1.5\text{--}3\sigma$. All limits are 2σ . The dashed lines show the expected ratios assuming power-law approximations for the infrared, sub-mm, and radio emission. The top dashed line represents an infrared-warm ULIRG, while the lower dashed line represents an infrared-cool ULIRG. Redshift estimates are shown by the dotted lines. The observed ratios are consistent with the SEDs of local ULIRGs at the expected redshifts of $z \sim 1\text{--}4$ for the SMG population. Strong radio galaxies which do not obey the far-infrared to radio correlation are located in the lower-left.

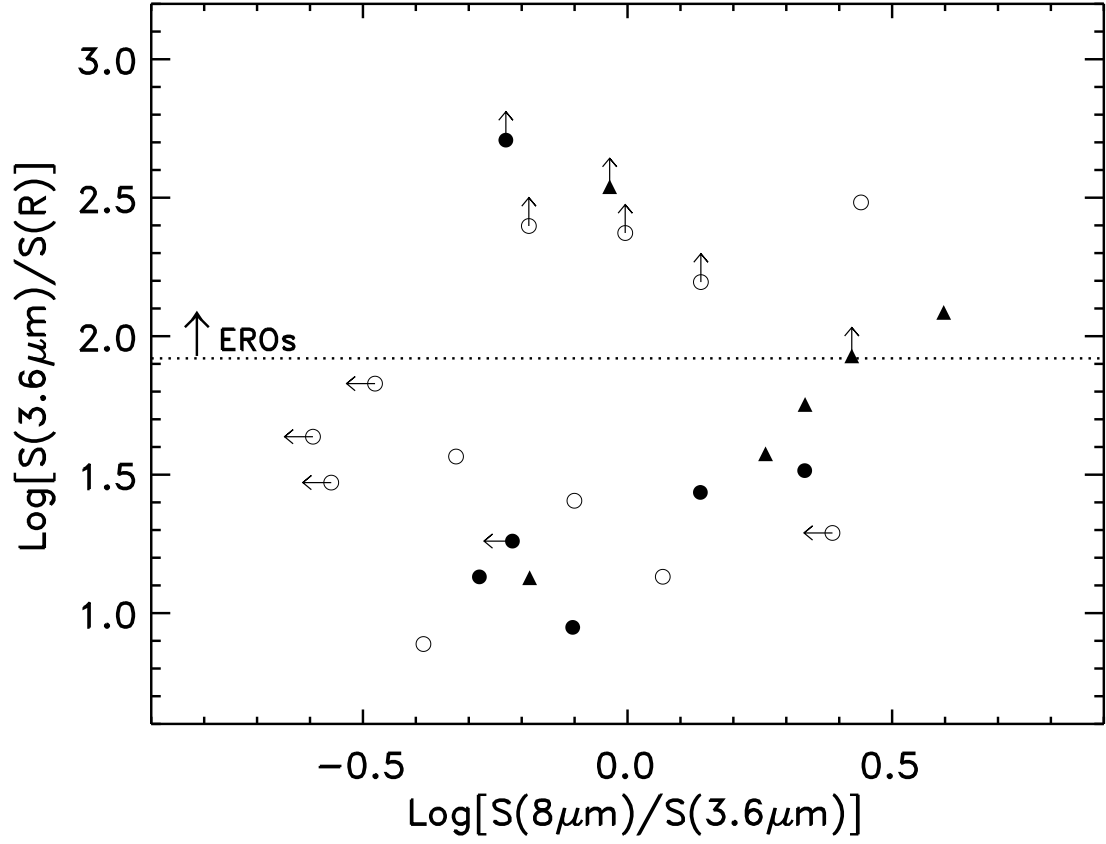


Fig. 3.— The S3.6/S(R-band) flux density ratios as a function of IRAC color given by the S8/S3.6 flux density ratio for sources with detections at $3.6\mu\text{m}$. Symbols are the same as Figure 1. EROs are located above the dotted line, corresponding to $R - [3.6] > 7.5$ (or $R - K > 6$). The data show a wide range of IRAC colors.

Table 1. FLSV Radio-Selected Candidate Submillimeter Galaxies

(1) Source	(2) Position $\alpha(J2000) \delta(J2000)$	(3) S(1.4GHz) (μ Jy)	(4) S(850 μ m) (mJy)	(5) S24 (μ Jy)	(6) R-band (mag)	(7) S3.6 (μ Jy)	(8) S4.5 (μ Jy)	(9) S5.8 (μ Jy)	(10) S8.0 (μ Jy)	(11) submm $\frac{(1+z_{phot})}{(T_d/40K)}$	(12) IRAC ($1+z_{phot}$)	(13) Notes
1	17:18:12.9+59:39:22	750 ± 120	7.0 ± 2.3	2750 ± 280	19.68 ± 0.05	559 ± 56	365 ± 37	362 ± 36	293 ± 29	2.3 ± 0.8	< 2.5	a
44	17:17:29.7+59:54:29	74 ± 9	9.9 ± 2.9	399 ± 40	23.44 ± 0.10	4.4 ± 0.8	...	b
48	17:17:33.7+59:53:56	54 ± 9	13.1 ± 2.9	232 ± 28	23.83 ± 0.11	16.5 ± 1.7	18.0 ± 1.8	14.9 ± 3.3	< 10	5.0 ± 0.8	3 ± 0.8	
115	17:17:43.4+59:48:03	262 ± 26	5.4 ± 1.6	373 ± 37	24.72 ± 0.20	13.0 ± 1.3	13.0 ± 1.3	< 10.0	28.1 ± 3.3	2.8 ± 0.8	...	
119	17:17:12.7+59:47:53	81 ± 9	10.2 ± 2.8	146 ± 28	> 26.4	43.3 ± 4.3	44.0 ± 4.4	42.9 ± 4.3	25.5 ± 3.3	4.3 ± 0.8	3 ± 0.8	c
199	17:17:29.4+59:41:13	116 ± 12	7.5 ± 2.5	301 ± 30	23.44 ± 0.14	35.4 ± 3.5	39.9 ± 4.0	49.3 ± 4.9	48.6 ± 4.9	3.7 ± 0.8	...	$z = 1.06^d$
208	17:18:10.9+59:40:41	77 ± 9	6.8 ± 1.9	78 ± 28	22.62 ± 0.10	24.5 ± 2.5	24.0 ± 2.4	< 10	19.3 ± 3.3	3.9 ± 0.8	...	
45A	17:17:47.5+59:54:24	80 ± 9	7.2 ± 2.5	200 ± 28	24.12 ± 0.14	26.0 ± 2.6	27.4 ± 2.7	36.5 ± 3.7	47.4 ± 4.7	4.0 ± 0.8	...	e
47	17:17:22.5+59:54:12	100 ± 10	4.9 ± 2.4	498 ± 50	25.31 ± 0.22	28.2 ± 2.8	45.6 ± 4.6	68.1 ± 6.8	111.6 ± 11.2	3.4 ± 0.8	...	c,f
73	17:17:57.9+59:52:00	118 ± 12	5.8 ± 2.1	135 ± 28	> 26.4	29.4 ± 2.9	35.5 ± 3.6	30.7 ± 3.3	27.2 ± 3.3	3.4 ± 0.8	3 ± 0.8	c
139	17:18:23.2+59:45:53	215 ± 22	5.0 ± 2.8	444 ± 44	22.62 ± 0.05	36.9 ± 3.7	32.5 ± 3.3	27.9 ± 3.3	24.1 ± 3.3	2.9 ± 0.8	< 2.5	
145	17:17:46.2+59:45:17	66 ± 9	8.7 ± 4.0	161 ± 28	> 26.4	7.2 ± 1.0	7.7 ± 1.0	< 10	19.1 ± 3.3	4.3 ± 0.8	...	c
156	17:18:16.8+59:44:30	82 ± 9	4.4 ± 2.5	368 ± 37	25.64 ± 0.37	9.7 ± 1.0	12.9 ± 1.3	25.0 ± 3.3	21.0 ± 3.3	3.5 ± 0.8	3.5 ± 0.8	
191	17:17:15.5+59:42:02	145 ± 15	3.8 ± 2.5	277 ± 28	25.35 ± 0.34	< 3	< 3	< 10	< 10	3.0 ± 0.8	...	
75	17:18:01.7+59:51:47	38 ± 9	< 7.5	416 ± 42	> 26.4	20.0 ± 2.0	24.6 ± 2.5	27.2 ± 3.3	19.8 ± 3.3	< 4.8	3.5 ± 0.8	c
79A	17:17:22.8+59:51:30	114 ± 11	< 6.6	408 ± 41	23.30 ± 0.17	54.2 ± 5.4	38.9 ± 3.9	36.6 ± 3.7	25.7 ± 3.3	< 3.6	< 2.5	g
85	17:18:12.3+59:50:56	44 ± 9	< 8.4	< 84	21.93 ± 0.05	40.1 ± 4.0	26.4 ± 2.6	23.9 ± 3.3	16.5 ± 3.3	< 4.7	< 2.5	
91	17:17:43.7+59:50:22	43 ± 9	< 7.8	331 ± 33	> 26.4	13.3 ± 1.3	17.9 ± 1.8	15.5 ± 3.3	18.3 ± 3.3	< 4.7	...	c
99	17:17:06.4+59:49:25	139 ± 14	< 8.4	< 84	23.50 ± 0.15	36.3 ± 3.6	25.3 ± 2.5	10.0 ± 3.3	< 10	< 3.6	< 2.5	h
108	17:17:41.2+59:48:36	1080 ± 130	< 8.1	< 84	> 26.4	< 3	< 3	< 10	< 10	< 2.2	...	
109	17:17:38.5+59:48:32	765 ± 110	< 6.6	< 84	24.19 ± 0.14	< 3	< 3	< 10	< 10	< 2.2	...	
128B	17:17:47.0+59:47:12	62 ± 9	< 9.0	< 84	25.41 ± 0.26	4.1 ± 1.0	3.6 ± 1.0	< 10	< 10	< 4.4	...	i
155	17:17:56.0+59:44:32	60 ± 9	< 7.2	< 84	24.60 ± 0.27	30.0 ± 3	32.7 ± 3.3	21.7 ± 3.3	< 10	< 4.3	3 ± 0.8	
136	17:17:11.6+59:46:21	108 ± 9	< 6.9	292 ± 29	23.89 ± 0.16	21.8 ± 2.2	23.5 ± 2.4	19.0 ± 3.3	17.3 ± 3.3	< 3.7	3 ± 0.8	
146	17:18:12.9+59:44:54	627 ± 63	< 9.9	217 ± 28	23.83 ± 0.10	39.3 ± 3.9	27.4 ± 2.7	15.7 ± 3.3	< 10	< 2.6	< 2.5	
150	17:17:42.4+59:44:56	68 ± 9	< 6.9	259 ± 28	23.37 ± 0.14	18.7 ± 1.9	11.8 ± 1.2	< 10	21.8 ± 3.3	< 4.1	...	$z = 0.84^d$
198	17:17:21.4+59:41:13	114 ± 12	< 8.1	< 84	> 26.4	21.2 ± 2.1	22.0 ± 2.2	13.3 ± 3.3	13.8 ± 3.3	< 3.7	< 2.5	c
211	17:18:21.3+59:40:27	356 ± 36	< 8.4	432 ± 43	26.16 ± 0.42	32.3 ± 3.2	41.7 ± 4.2	60.1 ± 6.0	89.2 ± 8.9	< 2.9	...	c

Note. — (1)Radio source identifier. (2)Radio positions which are accurate to about $\pm 2''$. (3)Radio flux densities from the Westerbork and VLA data. (4)SCUBA 850 μ m measurements. Sources 1–208 have $> 3\sigma$ 850 μ m detections. Sources 45A–191 have 1.5–3 σ 850 μ m measurements, and sources 75–211 are non-detections at 850 μ m. All flux density and magnitude limits are given as 3σ . (5)MIPS-24 μ m measurements. (6)Optical R-band magnitudes from NOAO 4m. (7)–(10)IRAC flux densities. (11)Photometric redshift estimate of $(1+z) \times (T_d/40K)^{-1}$ based on the sub-mm to radio relationship of Carilli & Yun (1999), accounting for the degeneracy

of redshift and dust temperature in the relationship (Blain et al. 1999). (12) Photometric redshift based on the assumed rest-frame $1.6\mu\text{m}$ peak in the IRAC SED. (a) Measurements summed over all five components (Fig. 1). Source 1 is also detected at longer wavelengths with $S_{70} = 30 \pm 6 \text{ mJy}$ and $S_{160} = 130 \pm 26 \text{ mJy}$. Sources not detected in the $70\&160\mu\text{m}$ MIPS-bands have 3σ limits of about $< 10\&< 50 \text{ mJy}$, respectively. (b) Detected in IRAC-bands, but IRAC measurements are confused with nearby bright optical source. (c) ERO based on high $S_{3.6}/S_{\text{R}}$ flux density ratio. (d) Spectroscopic redshift based on Keck DEIMOS data (Choi et al. 2004). (e) Brighter radio component 45A has $24\mu\text{m}$ counterpart and is adopted as the primary counterpart, since 45B has no associated $24\mu\text{m}$ source. (f) Detected in MIPS-70 with $S_{70} = 13 \pm 3 \text{ mJy}$. (g) Brighter radio component 79A has a $24\mu\text{m}$ counterpart and ‘merger-like’ morphology with two optical components. (h) Source 99 has two optical components showing a merger-like morphology. (i) Neither radio component of source 128 has a $24\mu\text{m}$ counterpart; 128B is adopted as the counterpart for flux density comparisons since there are no optical or IRAC counterparts associated with 128A.